*universe*

MDPI

*Article*

# On the Nucleosynthetic Origin of Presolar Silicon Carbide X-Grains

**Waheed Akram [1,2,*], Oliver Hallmann [2,3], Bernd Pfeiffer [2] and Karl-Ludwig Kratz [2,3]**

[1] Department of Earth Sciences, University of Oxford, Oxford OX1 3AN, UK
[2] Department of Chemistry, Johannes Gutenberg University of Mainz, D-55128 Mainz, Germany
[3] Max-Planck Institute for Chemistry, Otto-Hahn Institute, D-55128 Mainz, Germany
* Correspondence: waheed.m.akram@gmail.com

**Abstract:** In this paper we present an extension of our nucleosynthesis parameter study within the classical *neutrino-driven wind* scenario of core-collapse supernovae (ccSNe). The principal aim of this decade-old study was to shine light on the production of the historical 'p-only' isotopes of the light trans-Fe elements in the Solar System (S.S.). One of our earliest key findings was the co-production of neighbouring classical 's-only' and 'r-only' isotopes between Zn (Z = 30) and Ru (Z = 44), alongside the synthesis of light p-isotopes, under similar conditions of a moderately neutron-rich, low-entropy, charged-particle component of Type II SNe wind ejecta. We begin this analysis by expressing the need for nuclear-structure input from detailed spectroscopic experiments and microscopic models in the relevant shape-transition mass region between N = 50 and N = 60. Then, we focus on the unique nucleosynthetic origin of the anomalous isotopic compositions of Zr (Z = 40), Mo (Z = 42) and Ru (Z = 44) in presolar silicon carbide X-grains. In contrast to the interpretation of other studies, we show that these grains do not reflect the signature of a 'clean' stellar scenario but are mixtures of an exotic rapid (r-process like) nucleosynthesis component and different fractions of S.S. material. Thus, the synthesis of these light isotopes through a 'primary' production mode provides further means to revise the abundance estimates of the light trans-Fe elements in the S.S., reducing our dependence on still favoured 'secondary' scenarios like Type Ia SNe or neutron-bursts in exploding massive stars.

**Keywords:** neutrino-driven wind; type II supernovae; r-process; nuclear shell structure; cosmochemistry; presolar grains

check for updates

**Citation:** Akram, W.; Hallmann, O.; Pfeiffer, B.; Kratz, K.-L. On the Nucleosynthetic Origin of Presolar Silicon Carbide X-Grains. *Universe* **2022**, *8*, 629. https://doi.org/10.3390/universe8120629

Academic Editor: Sara Palmerini

Received: 15 June 2022
Accepted: 14 November 2022
Published: 28 November 2022

**Publisher's Note:** MDPI stays neutral with regard to jurisdictional claims in published maps and institutional affiliations.

**Copyright:** © 2022 by the authors. Licensee MDPI, Basel, Switzerland. This article is an open access article distributed under the terms and conditions of the Creative Commons Attribution (CC BY) license (https://creativecommons.org/licenses/by/4.0/).

## 1. Introduction

Advances in nuclear astrophysics have always benefited from the rich and complex interplay between the findings of the nuclear physics, astronomy and astrophysics, and cosmochemistry communities. Notable examples of such discoveries from the early days include the detection of Technetium in S-stars [1], and the solar/cosmic abundance curves derived from early solar system (S.S.) materials [2,3], both of which helped to influence the seminal publications on nuclear astrophysics by Burbidge et al. [4] and Cameron [5] in the 1950s. More recent measurements of the elemental abundances in metal-poor stars alongside the isotopic compositions of primitive whole-rock meteorites and meteoritic inclusions strongly suggest the existence of a multitude of nucleosynthetic processes synthesizing elements heavier than iron (Fe), going beyond the three classical p-, s- and r-processes originally proposed by [4]. This has generated considerable interest, especially in the synthesis of stable isotopes in the mass region from the tail end of the Fe-group elements around Zn (atomic number Z = 30), passing the first s-process peak ($38 \leq Z \leq 40$), running up to Cd (Z = 48)—a region traversing the spheres of charged-particle and neutron-capture nucleosynthesis. Varying nucleosynthetic contributions from (i) the p-process (e.g., [6,7]), (ii) the weak s-process, ([8,9] and references therein) and (iii) the weak r-process ([10–12] and references therein) are often evoked to explain nucleosynthesis in this mass region (in addition to quasiequilibrium $\alpha$-rich freezeout).

The *elemental* abundance patterns observed in metal-poor halo stars (e.g., [13–16]) have revived and intensified various theoretical studies of nucleosynthesis models within this mass range [16–32]. Further incentives for exploring the multi-faceted nature of nucleosynthetic processes in this domain arise from the *isotopic* analyses of refractory inclusions and presolar grains—commonly referred to as stardust—embedded within defined classes of primitive meteorites (e.g., [33–37]). Millimeter to cm-sized refractory inclusions such as Ca,Al-rich inclusions (CAIs)—high-temperature condensates that formed in the early S.S.—represent complex and variable admixtures of materials having a largely solar composition alongside a minor presolar component, which potentially comprise several presolar phases originating from *multiple* nucleosynthetic and/or astrophysical sources. Each of the nm to µm-sized presolar grains, on the other hand, were formed entirely within or around the atmosphere of a *single* stellar source. As a result each grain sampled nucleosynthetic material exclusively from a unique stellar environment [38]. The remarkable preservation of these grains in meteorites thus ensures that their chemical compositions reflect directly the compositions of the stellar system(s) where these grains condensed, thereby yielding information about nuclear processes taking place in the associated stellar interiors and mixing episodes bringing freshly synthesized material up to the stellar surface [39].

The best studied of all presolar grains are silicon carbide (SiC) grains, the majority of them known as *mainstream* or s-process grains, which formed around asymptotic giant branch (AGB) stars (a more in-depth discussion of SiC grains is provided in Section 5.1). Arguably more interesting but definitely more enigmatic are the rare subclass of Type-X grains (SiC-X) [34,40] whose light trans-Fe isotopic compositions—e.g., Zr (Z = 40), Mo (Z = 42) and Ru (Z = 44)—have evaded a straightforward p-, s- or r-process origin, necessitating alternate nucleosynthesis scenarios for these elements (see Section 5.2 for more). Popular among these scenarios is the 'secondary' (i.e., metallicity dependent) neutron-burst occurring in the shocked He-shell of exploding massive stars [41,42]. However, one characteristic trait of all of these proposed models is that they are unable to co-produce *all* the light p-, s- and r-process isotopes as observed in SiC-X grains, or even in S.S. proportions in general (especially for the two most abundant p-isotopes $^{92}$Mo and $^{94}$Mo).

In this article we present an alternate nucleosynthesis model based on updates of our earlier preliminary results [31,43,44] from the classical core-collapse supernova (ccSN), low-entropy, neutrino-driven-wind scenario. We show that our model is able to (1) synthesize the light trans-Fe elements between Zn and Ru in respectable quantities by means of a 'primary' process highlighting the importance of charged-particle reactions, and (2) explain the anomalous Zr, Mo and Ru isotope signatures reported for SiC-X grains using a single set of consistent model parameters for entropies and electron fractions, thereby providing a solution to the nucleosynthetic and astrophysical origins of SiC-X grains.

This article is structured as follows: we briefly introduce the astrophysical model used for our nucleosynthesis calculations in Section 2 and highlight the importance of having unified nuclear data input for nuclear structure calculations in Section 3, followed by our model predictions for the synthesis of Zr, Mo and Ru isotopes in Section 4. This leads on to the discussion of SiC-X grains in Section 5, focusing on their discovery, classification and anomalous Zr, Mo and Ru isotope compositions. We conclude by analysing the corresponding Zr, Mo and Ru isotope yields from various nucleosynthetic models—including our own neutrino-driven wind model—to find the model that best explains the anomalous SiC-X grain data in Section 6.

## 2. Parametric Core-Collapse Supernova Neutrino-Driven Wind Model

The nucleosynthesis calculations used in this study were performed with the Basel code of [45] (with upgrades from [46,47]) and are based on the 'neutrino-driven wind' model of core-collapse supernovae as outlined in [20,21,48]. Although we adopt a *site-independent* r-process model parameterized by neutron density $n_n$ and temperature $T$, we show [31] that this can be translated into a specific *astrophysical* model (e.g., neutrino-driven wind) when the parameters are considered as macro-physical quantities. The neutrino-driven

wind refers to the ejected mass layers—just above the newly formed proto-neutron star following core collapse—that are driven out by the neutrinos. Owing to the extremely high matter density in such an environment, a significant portion of the neutrinos emanating from the neutron star interact with the photodisintegrated matter in those mass layers, predominantly consisting of protons and neutrons, altering the proton-to-neutron ratio and by extension the electron fraction ($Y_e = Z/A$). During core collapse, the entropy ($S$) of matter in the core decreases whilst increasing for mass shells further away from the surface of the neutron star. The equation of state (EOS) of matter within the neutrino-driven wind is based on the *entropy per baryon* (as a thermodynamic state function), which assumes the role of neutron density in the classical r-process model: the higher the entropy, the more neutrons per seed nuclei $Y_n/Y_{seed}$. For a hot gas with temperatures exceeding $T_9 \sim 9$ (where $T_9 \equiv T/10^9$ K), the entropy will be dominated by radiation with an additional fermionic contribution from relativistic electrons and positrons.

During the expansion of the initial hot bubble the temperature continues to decrease and drops below $T_9 \sim 6$, so that the α-particles can start to react with each other to form $^{12}$C, either following the triple-α reaction

$$3\alpha \rightarrow {}^{12}C \tag{1}$$

or if neutrons are available, by the three-body reaction

$$\alpha + \alpha + n \rightarrow {}^{9}Be \tag{2}$$

followed by the reaction

$$^{9}Be(\alpha,\ n)^{12}C \tag{3}$$

Both Equations (1) and (2) depend on the square of the matter density (ρ); whereas reaction (2) depends also on the electron fraction ($Y_e$) which corresponds to the proton-to-nucleon ratio. In the neutrino-driven wind model, we assume entropies at least of the order of 1 $k_B$ per baryon, reflecting low matter densities (since $S \propto T^3/\rho$ [31]). In this case, the reaction channels (Equations (1) and (2)) are less effective resulting in a so-called 'α-rich freezeout' with a considerable amount of α-particles and neutrons left over at $T_9 \sim 3$. For higher matter densities, i.e., very low entropies ($S < 0.1$), the three-body reactions (1) and (2) are effective and lead to a total recombination of α-particles and free neutrons. During this recombination phase, called 'normal freezeout', no subsequent neutron-capture process is possible due to the lack of free neutrons.

The final abundances for an α-rich charged-particle freezeout at around $T_9 \sim 3$ are dependent on $Y_e$, yielding seed nuclei dominated by Fe-group elements for higher $Ye$ (just below 0.5) up to seed nuclei with $A \approx 100$ for low $Y_e$ of 0.4. Under such conditions of a primary charged-particle process with entropies at least high enough to warrant an α-rich freezeout, the co-production of light trans-Fe p-, s- and r-process isotopes will occur, which we will discuss later in detail for the presolar SiC-X grains (Section 4).

With gradually decreasing $Y_e$ and increasing $S$, the neutron-to-seed ratio $Y_n/Y_{seed}$ increases and can be seen as a measure of the 'strength' of the r-process in neutrino-driven winds ($Y_n/Y_{seed} \propto V_{exp}(S/Y_e)^3$; where $V_{exp}$ is the expansion velocity of the ejecta [31]). As a typical example, for a moderate $Y_e = 0.45$ (which corresponds to a matter composition of 45% protons and 55% neutrons) a neutron-capture process will start at the minimum conditions of $Y_n/Y_{seed} \sim 1$ and $S \sim 100$. For a more detailed breakdown of the delineation of nucleosynthesis in the neutrino-driven wind into distinct modes—(a) α-rich freezeout, (b) neutron-rich α-freezeout, (c) 'weak' r-process and (d) 'main' r-process—within varying entropy ranges, and a tabulation of the stable isotope yields under these respective conditions, the curious reader may refer to the text (and Table 1) in [31].

## 3. Nuclear Data Input—A Unified Approach

In general, the observed abundance patterns of the trans-Fe elements (i.e., of the historical p-, s- and r-processes) are the result of successive nuclear reactions along their respective process pathways. Hence, apart from stellar parameters the abundance patterns also depend on a wide range of nuclear properties with quite different $N/Z$ ratios. For calculations of the ccSN scenario discussed in this paper, of major importance are the ground-state masses (to be more precise, their derivatives of the neutron-binding energies $S_n$ and the reaction $Q$ values), beta-decay properties (i.e., half-lives $T_{\frac{1}{2}}$ and beta-delayed neutron-emission ($\beta$dn) probabilities $P_n$), as well as the relevant reaction cross-sections (here in particular the neutron-capture rates $\sigma(n,\gamma)$).

Before presenting a detailed discussion of the nuclear-data input used in our ccSN neutrino-driven wind calculations, we would like to highlight an inherently critical issue. This concerns the wealth of different nuclear quantities required for nucleosynthesis calculations and the difficulty encountered in acquiring these quantities from a single source, even today. Obtaining them from different sources, however, usually raises questions of consistency. Additionally, in such heterogeneously sourced calculations, especially for nuclear masses and beta-decay properties, astrophysically relevant nuclear-structure quantities may occasionally vanish or 'artificial' effects will appear, strongly limiting the predictive power far from beta-stability.

In light of the above consideration, from the beginning of our attempts to model the r-process (e.g., [17,49]), our nuclear-structure calculations have predominantly used the continually updated finite range droplet model/quasi–particle–random–phase–approximation (FRDM/QRPA) framework of [19,50–56], in which all nuclear properties can be studied in a self-consistent way. Aware that this approach must have its deficiencies as well, we have continuously improved our nuclear-structure data sets, e.g., by including the beta-strength function calculations on top of the Gamow-Teller (GT) mode and the first-forbidden (ff) transitions from the Gross theory kindly provided by Takahashi [57], whilst also taking into account upcoming experimental nuclear data, and known local nuclear-structure properties–either (model-inherent) not contained or incorrectly described by the above FRDM/QRPA approach. Gamma-ray spectroscopy experiments [58–66] have shown that such an impaired model performance may occur, in particular, in shape-transition areas. For the case of the light trans-Fe elements this concerns the spherical N = 56 subshell closure of neutron-rich isotopes in the region Z = 34 (Se) to Z = 42 (Mo), where most global (macroscopic)-microscopic mass models incorrectly predict ground-state (g.s.) deformation. This leads partly to drastic differences in the theoretical beta-strength functions, and consequently also in the related integral beta-decay properties $T_{\frac{1}{2}}$ and $P_n$.

As an illustrative example we choose here the well-known spherical isotope $^{92}$Rb (Z = 37, N = 55) with $T_{\frac{1}{2}}$ = 4.5 s and its low $P_n$ = 0.01% [56]. In contrast to experimental results, the global FRDM/QRPA predicts a prolate ground state deformation of $\varepsilon_2$ = 0.22, where the valence neutron occupies the [411]3/2 Nilsson orbital of $d_{5/2}$ single-particle origin. The GT decay of the $3/2^+$ mother isotope then leads to the low-lying [440]1/2, [431]3/2 and [433]5/2 proton orbitals of $g_{9/2}$ single-particle origin in the deformed daughter nucleus $^{92}$Sr. The $(Q\text{-}E)^5$ weighting of the Fermi function, then results in a very short $T_{\frac{1}{2}}$(GT) = 271 ms, which is a factor of 16.6 lower than the experimental value. When performing the GT strength calculations with the standard QRPA model for the known spherical system, the results for the $T_{\frac{1}{2}}$ and $P_n$ values are not at all satisfactory either. The GT decay of the valence neutron in the $d_{5/2}$ single-particle level will now find no proton single-particle partner for the Z = 38 $^{92}$Sr daughter below its $S_n \approx 7.3$ MeV. As shown in the top subplot of Figure 2 in Möller, Pfeiffer and Kratz (2003) [56], this will consequently lead to a much longer $T_{\frac{1}{2}}$(GT) = 1.3 h (which is three orders of magnitude higher than the experimental value), and in addition a $P_n$ value close to 100%. At this point, our two model enhancements to the pure GT decay come into play [56]. The first one is an empirical beta-strength function [58]. As is shown in the middle subplot of Figure 2 in Möller, Pfeiffer

and Kratz (2003) [56], in the case of $^{92}$Rb where the lowest GT transition sits just above $S_n$, this spreading shifts part of the original GT 'spike' down to the neutron-bound region of the spectrum. This results in a lowering of both $T_{\frac{1}{2}}$ by a factor of 6.5 to about 12 min (which is now still roughly a factor of 170 above the experimental value) and the $P_n$ value by a factor of 20 (which is still roughly a factor 400 too high). In the second of our shell-model improvements, we account for the effect of the first-forbidden strength taken from the positive parity $\nu$-$d_{5/2}$ to the negative-parity $\pi$-$f_{5/2}$ single-particle level. As indicated in the low subplot of Figure 2 in Möller, Pfeiffer and Kratz (2003) [56] the 'final' $T_{\frac{1}{2}}$(GT + ff) is further lowered to about 8.5 s (which is now only slightly higher by a factor of 1.9 than the experimental value), and the $P_n$ value also drops to an acceptable value of 0.05%.

In the light trans-Fe region relevant in particular for the Zr, Mo and Ru isotopes of the presolar SiC-X grains, we have systematically replaced the predicted g.s. deformations with spherical shape for the $52 \leq N \leq 59$ isotopes of Z = 34 (Se) up to Z = 39 (Y). For nearly all of these isotopes our improved FRDM/QRPA calculations yield longer $T_{\frac{1}{2}}$(GT+ff) for spherical g.s. shapes than for the originally predicted deformed shapes. The most extreme (spher./def.) factors occurred for the N = 55 isotones $^{89}$Se ($f$ = 12.7), $^{90}$Br (18.0), $^{91}$Kr (23.1), $^{92}$Rb (31.6) and $^{93}$Sr (52.7).

Reaction rates, in particular neutron-capture cross-sections, $\sigma(n,\gamma)$, can be calculated with statistical models (here the average continuum Hauser-Feshbach (HF) model), as long as nuclear level densities in the compound nucleus are sufficiently high to justify such averaging approaches. This method requires knowledge of several relevant nuclear quantities (e.g., optical potentials, giant dipole resonance parameters for gamma widths, level density parameters, reaction Q values, correct g.s. spins of the reaction mother and compound nuclei) either from experiment (e.g., [49,56,66,67]) or from theory (e.g., [68–72]). Contrary to neutron-induced reactions, where the astrophysical applicability can be directly derived from the level density, for charged-particle induced reactions the Coulomb barrier must also be taken into account. By folding the Maxwell-Boltzmann velocity distribution of the projectiles at a given temperature with the penetrability through the barrier, the so-called Gamow window can be derived, in which most of the reactions will take place. The location and width of the Gamow peak depend on the charges of projectile and target, and on the temperature.

For nuclei near closed neutron shells, the level density is lower and the HF approach may not be applicable. It should then be replaced by the Breit-Wigner (BW) resonance states plus direct-capture (DC) contributions (e.g., [73–76]). For neutron-capture on long-lived isotopes ($T_{\frac{1}{2}} > 1$ d) we may use experiments with radioactive targets, and radioactive ion-beam experiments for shorter-lived nuclei. However, this is not the only way of studying neutron-unbound levels in radioactive nuclei. Depending on the decay energetics and the spins and parities involved, such states can also be populated via the 'inverse process' of neutron capture, i.e., β-delayed neutron-emission. For isotopes in the light trans-Fe region, the applicability of this inverse relationship was first documented for the compound nuclear states in $^{87}$Kr where three different spectroscopic methods [59,77,78] have been used, each having an impact on nuclear structure as well as astrophysical implications [66,67,79].

The first method [59] comprised neutron-capture and transmission measurements on the stable isotope $^{86}$Kr ($J^\pi = 0^+$) at the Oak Ridge electron linear accelerator (ORELA), where energies and neutron widths for 39 resonances above $S_n$ in the compound nucleus mboxtextsuperscript87Kr ($J^\pi = 5/2^-$) were determined. The second method [77] was a standard β-gamma decay study of radioactive $^{87}$Br ($J^\pi = 3/2^-$) performed at the OSIRIS (on-line separation of isotopes at a reactor in Studsvik) mass separator, where in addition to a detailed level scheme for the neutron-bound region, the gamma-de-excitation of 12 low-energy neutron-unbound $J^\pi = 5/2$ states were also observed. Additionally, the third method [78] was a high-resolution study of the β-delayed neutron spectrum of $^{87}$Br at the Mainz TRIGA (training research isotope production General Atomic) reactor, in which low-energy p-wave neutron-emission form $J^\pi = (1/2, 3/2)$ levels in $^{87}$Kr to the ground state of the final nucleus $^{86}$Kr were observed. With the observation of a one-to-one

correspondence of these $l_n = 1$ resonances with the respective $p_{\frac{1}{2}}$ and $p_{3/2}$ neutron-capture levels from $^{86}$Kr, the above postulated 'inverse relationship' between the two reactions was proven. While in the $^{86}$Kr(n,$\gamma$)$^{87}$Kr study of [59] all possible spins and parities are produced, from which experimental values for the total level density and the total neutron-capture cross-section can be derived, from the $^{87}$Br($\beta$)$^{87}$Kr(n)$^{86}$Kr decay mode only a BW resonance partial p-wave density and a partial $l_n = 1$ cross-section are obtained. When adding the $J^\pi = 5/2$ levels from the β-gamma study and then projecting the experimental partial $l_n = 1, 3$ level density onto the missing capture states not populated in β-decay, a reliable (lower-limit) estimate of the total cross-section is possible. In this way, from the high resolution β-delayed neutron energy spectra of $^{89-92}$Br measured at CERN/ISOLDE [80] as well as $^{92-97}$Rb at ILL/OSTIS [58,79,81,82], theoretical HF predictions of [83] were compared, and validated, with improved HF and BW reaction rates using experimental level density parameters deduced from Porter-Thomas fluctuation analysis [84,85] of the above βdn spectra.

## 4. Nucleosynthesis of Zr, Mo and Ru Isotopes in the Neutrino-Driven Wind

Our early parameter studies [31,43,44] within the neutrino-driven wind framework focused on understanding the origin of the p-isotopes $^{92,94}$Mo and $^{96,98}$Ru. These isotopes were found to occur for electron fractions $Y_e \geq 0.45$, where charged-particle (CP) reactions dominate for $S \leq 100$ and neutron-captures prevail for $S > 100$. As a natural extension of our early results, we continue to explore the nucleosynthesis of the neighbouring elements Zr, Mo and Ru under similar conditions ($Y_e = 0.45$), but with a finer parameter space grid. Sticking with the prototypical case of $Y_e = 0.45$ for illustrative purposes, we observe the co-production of all stable isotopes of Zr, Mo and Ru in considerable quantities (Figure 1, left panel; abundance plots). This includes the historical p-only ($^{92,94}$Mo, $^{96,98}$Ru), s-only ($^{96}$Mo, $^{100}$Ru) and r-only ($^{100}$Mo, $^{104}$Ru) isotopes. Although synthesis of these isotopes occurs over a wide range of entropies ($10 \leq S \leq 270\ k_B$/baryon), the bulk production of any given Zr, Mo or Ru isotope takes place in a narrow entropy band (Figure 1, right panel; cumulative abundance plots), corresponding to distinct nucleosynthesis modes.

*Zirconium*: over 80% of the stable isotopes of Zr are synthesized in the range $10 < S < 150$, with $^{90,91,92,94}$Zr almost entirely produced in the CP-component ($S < 100$).

*Molybdenum*: $^{92,94,96}$Mo are exclusively produced in the $S < 60$ region (CP-component), whereas higher entropy intervals are needed for $^{95,97,98}$Mo ($50 < S < 150$) corresponding to weak-r conditions, with $^{100}$Mo largely synthesized under weak-r conditions resembling more neutron-rich wind ejecta.

*Ruthenium*: as with Mo, the p-isotopes $^{96,98}$Ru are synthesized in the CP-region ($S < 50$), whereas $^{99,101,102,104}$Ru are wholly produced in the range $100 < S < 150$. Surprisingly, much higher entropies are needed for medium-mass $^{100}$Ru ($S \approx 200$, main r-conditions), which is shielded from the r-process production pathway by the practically stable isobar $^{100}$Mo. Only for very neutron-rich conditions (with exotic 'nearby' βdn emitting r-progenitors; mainly A ≈ 100, Rb and Kr isotopes), can the late re-capture of βdn's on long-lived (≈$10^5$ years) $^{99}$Tc increase the $^{100}$Ru abundance.

Further exploration of our models in the wider electron fraction range $0.4 \leq Y_e \leq 0.5$ gives qualitatively similar results and trends as those observed in Figure 1, with two key differences: (1) the total isotope yields of Zr, Mo and Ru generally decrease with higher $Y_e$, and (2) peak isotope production shifts to higher entropies with higher $Y_e$ (see [44]). Overall, all stable isotopes of Zr, Mo and Ru are produced under a very similar set of consistent astrophysical conditions characterized by a narrow $Y_e$-$S$ band within or close to the low-$S$, CP-component of ccSNe.

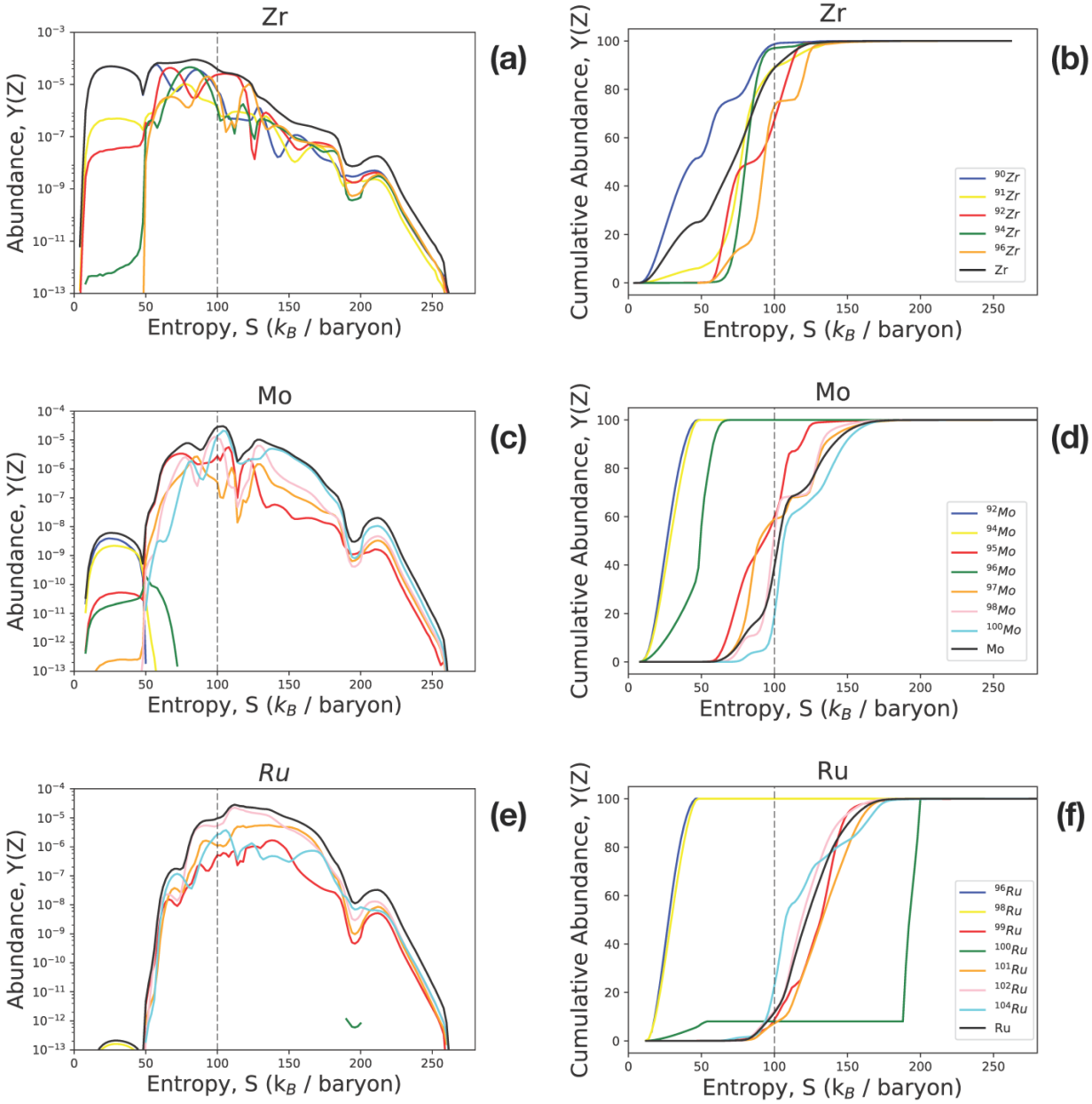



**Figure 1.** Isotope yields Y(Z) (**left panel**) and cumulative isotope yields (**right panel**) for Zr, Mo and Ru as a function of cumulative entropy (computed at $Y_e = 0.45$). Hypothetical boundary between charged-particle and neutron-capture domains (occurring at $S = 100\ k_B$/baryon for $Y_e = 0.45$) is indicated by vertical (dashed) line.

## 5. Observations from SiC-X Grains

### *5.1. Discovery and Classification of SiC-X Grains*

The laboratory analysis of presolar grains is often referred to as a 'new field of astronomy' [38] complementing the more well established analytical techniques of astronomical spectroscopy. However, the first experimental hints of the preservation of presolar grains date back to 1964 [86], eventually followed in 1987 by the actual discovery–that is, the isolation–of these grains from the fine-grained matrix of some of the least processed, undifferentiated chondrites (e.g., [87–90]). In all cases, presolar grains are recognized primarily by their highly anomalous isotopic compositions relative to the solar composition. For a comprehensive historical and scientific account of the tedious extraction methods used to isolate these grains from their host meteorites, and the subsequent high-sensitivity and

high-precision chemical analyses on such small sample sizes (individual grains), we refer the curious reader to [38] and the references within.

The study of presolar grains provides a wealth of information on a number of physical and chemical processes taking place in the stars and our own solar system, as recorded during the different stages of the life cycle of presolar grains. These include (1) *pre grain formation*, which holds clues to nuclear reactions taking place inside evolved stars (i.e., stellar nucleosynthesis and galactic chemical evolution); (2) *during grain formation*, which can shine light on the condensation and ejection of grains around circumstellar environments of evolved stars; and (3) *post grain formation*, where we may learn more about interstellar processes and early S.S. processes (e.g., molecular cloud collapse, accretion disk formation, incorporation of grains into meteorites) [91].

Today we know of several different types of presolar grains (e.g., silicon carbide, diamond, graphite, silicate, oxide; as classified by their major-element chemical compositions), each class thought to have originated in a different kind of evolved stellar environment (e.g., asymptotic giant branch stars, supernovae, novae, red giants). Each population of presolar grains is further broken down into subgroups, based on the differing isotopic signatures observed for these grains, reflecting the large variation of nucleosynthetic processes occurring in such environments. Silicon carbide (SiC) grains remain the best-studied type of presolar grain. This is largely due to a couple of factors–first, their highly refractory and chemically resilient nature, and second their relatively large grain sizes (0.1–20 μm) and abundances (~150 ppm) in their parent meteorite bodies. Isotopic analyses of the major-elements C, N, O and Si allow us to divide SiC grains into the following sub-populations: mainstream-, AB-, C-, X-, Y-, Z-, and nova-grains (see [38] for details). By far the largest subclass of SiC grains, constituting >90% of all SiC grains, are the *mainstream* grains, characterized by compositions (low $^{12}C/^{13}C$, high $^{14}N/^{15}N$ relative to S.S.) consistent with formation around thermally pulsating, low- and intermediate-mass asymptotic giant branch (AGB) stars. In stark contrast to mainstream grains are the rare (~1%) subclass of Type X grains (SiC-X; exotic) whose isotopic signatures (elevated $^{12}C$, $^{15}N$, $^{28}Si$ relative to S.S., alongside excesses of $^{26}Mg$, $^{44}Ca$ and $^{49}Ti$–from the decay of the radionuclides $^{26}Al$, $^{44}Ti$ and $^{49}V$, respectively) are more suggestive of explosive scenarios, like ccSNe [34,92]. Not surprisingly then the term supernova condensates, or SUNOCONS, has been used to describe SiC-X grains. Major-element compositions aside, SiC-X grains have attracted much attention with their heavy-element isotopic compositions–especially the light trans-Fe elements Zr, Mo and Ru–which have so far evaded a straightforward classical (i.e., p-, s-, r-) interpretation. Instead, these grains favour nucleosynthetic models intermediate between the s- and the r-process producing a 'rapid, but limited neutron dose' [34] such as those encountered in the neutron-burst models of [41,42].

### *5.2. Anomalous Zr, Mo and Ru Isotope Compositions of SiC-X Grains*

Almost 15 years ago, heavy-metal isotope compositions were reported for 12 individual SiC-X grains isolated from two different grain size fractions (KJG: 1.5–3 μm; KJH: 3–5 μm, [93]) of the carbonaceous chondrite Murchison (CM2 group) [33,34,94]. Grains of Type-X were identified using secondary ionization mass spectrometry (SIMS) [93] and subsequent heavy element (Fe, Sr, Zr, Mo, Ru, Ba) isotope compositions were measured using resonant ionization mass spectrometry (RIMS) on the Chicago-Argonne resonant ionization spectrometer for mass analysis (CHARISMA) [95]. Owing to small sample sizes and low elemental concentrations not all elements were analysed concurrently in all 12 grains.

Building on the results of that study [34], we focus here on an independent reanalysis and reinterpretation of the anomalous isotopic compositions reported for Zr (in four grains: 113-2, 113-3, 196-5, B2-05), Mo (in seven grains: 113-2, 113-3, 153-8, 133-1, 209-1, 100-2, B2-05) and Ru (in two grains: 322-1, H-2). Only for the three grains 113-2, 113-3, and B2-05 were concurrent measurements possible for both Zr and Mo (but not Ru). For completeness we also include data for the grain E2-10, which was included by the original

authors of the study [34] due to the resemblance of the Mo isotope compositions in this grain with the seven other SiC-X grains where Mo was also measured. For reasons of brevity and the increased robustness of the Mo isotope data, we limit our discussion to the analysis and interpretation of Mo isotopes, referencing Zr and Ru where appropriate. The isotopic data [34] are reported as ratios ($^{i}x/^{k}x_{S}$, s: sample)—normalized to a base isotope or normalization isotope ($^{k}x$)—and are expressed as deviations from the terrestrial (≈solar, ($^{i}x/^{k}x$)) composition in parts per thousand, denoted $\delta^{i}x_{k}$, as defined by Equation (4) following the usual nomenclature from cosmochemistry.

$$\delta^{i}x_{k} = \left[ \frac{\left(^{i}x/^{k}x\right)_{S}}{\left(^{i}x/^{k}x\right)_{\odot}} - 1 \right] \times 10^{3} \quad (4)$$

The choice of normalization isotope is non-trivial and is usually between the most naturally abundant isotope (reducing the overall statistical uncertainty in all derived isotope ratios, i.e., to obtain high counting statistics) and the isotope with the fewest isobaric interferences (minimizing systematic uncertainties, i.e., to make fewer background corrections to the data). Complex datasets, however, can benefit from the analysis of multiple normalization schemes, each one revealing different characteristics of the underlying nature of the isotopic signature observed. For instance, for the purposes of understanding the nucleosynthetic origins of SiC-X grains, we may renormalize the data relative to 'clean' p-, s-, or r-only isotopes to make the interpretation easier.

*Molybdenum*: Under the original normalization to $^{96}$Mo (s-only) [34], SiC-X grains display, on *average*, depletions in p-isotopes (i.e., $\delta^{92}Mo_{96}$, $\delta^{94}Mo_{96} < 0$), large enrichments in the n-capture isotopes (i.e., $\delta^{95}Mo_{96}$, $\delta^{97}Mo_{96}$, $\delta^{98}Mo_{96} > 0$) and only slight or zero variations for the most neutron-rich isotope (i.e., $\delta^{100}Mo_{96} \approx 0$), all relative to solar. Further insight into the nucleosynthetic signatures of these grains is gained by recasting the δ-values into *absolute* ratios (by rearranging Equation (4)); these absolute ratios we may compare directly with isotope ratios calculated using the isotopic yields from stellar models. For instance, renormalizing to $^{97}$Mo we see that—relative to S.S.—the classical p-isotopes ($^{92,94}$Mo) and r-isotope ($^{100}$Mo) in SiC-X grains are depleted and the largely s-isotopes ($^{95,98}$Mo) are enriched by a factor of two, whereas the s-only isotope ($^{96}$Mo) is present in identical abundances as $^{97}$Mo.

*Zirconium*: Renormalizing the Zr isotope data to $^{90}$Zr—and once again looking at the absolute ratios—we find that the SiC-X grains are characterized by depletions relative to $^{90}$Zr ($0.2 \leq {}^{i}\mathrm{Zr}/90\mathrm{Zr} \leq 0.5$; $i$ = 91, 92, 94, 96), relative to solar.

*Ruthenium*: The Ru isotope data are more complex and the analysis hindered by the fact that Ru isotope data are only reported for two SiC-X grains, with relatively large measurement uncertainties. Renormalizing to $^{101}$Ru, we find that the lighter mass isotopes ($^{96,98,99,100}$Ru) are on *average* under-abundant relative to $^{101}$Ru, whereas $^{104}$Ru occurs in similar proportions to $^{101}$Ru, and $^{102}$Ru is over-abundant to $^{101}$Ru by a factor of two, all relative to solar.

The results of the various normalizations presented here reiterate the earlier observation of [34,40,94] that SiC-X grains display complex, non-classical p-, s-, r-process signatures. To help make more sense of the data we adopt standard methods of geochemistry and cosmochemistry for analyzing isotope variations: *three-isotope plots* and *mixing lines* (e.g., see [96]). These techniques allow us to simultaneously analyse more than one pair of isotope ratios, thereby constituting a form of two (or n-) dimensional analysis that proves to be more meaningful and constraining than the analysis of individual isotope ratios (one-dimensional analysis). Consequently, these abstractions (i.e., mixing lines) allow us to (1) identify and quantify any isotopic correlations amongst the measured grains, (2) ascertain possible common origins of the grains, and (3) recognize grains as either pure stellar components/material (i.e., end members) or as chemical admixtures of isotopically distinct end members—not necessarily all stellar. Figure 2 (left plot) shows a three-isotope plot for Mo with $^{96}$Mo/$^{97}$Mo plotted against $^{92}$Mo/$^{97}$Mo in two-dimensional space. Normalization

to the same base isotope, in this case $^{97}$Mo, is an essential feature of three-isotope plots to ensure consistency during the analysis. The Mo isotope data for the SiC-X grains define a linear trend ($r^2$ = 0.91) characterised by the grain B2-05 at one extreme (ignoring E2-10 for the moment) and the Earth (or solar material, S.S.) diametrically opposite at the other extreme (overlooking the relatively large uncertainties on grain 209-1). The same linear correlation is observed for Zr (see Figure 2 (right plot): $^{91}$Zr/$^{90}$Zr vs. $^{92}$Zr/$^{90}$Zr, $r^2$ = 0.83), also with the same two isotopic end-components: S.S. and B2-05. These trends are best interpreted as SiC-X grains being admixtures of two—and *strictly* two—isotopically distinct components, thereby suggesting a common origin for this set of grains (a result already recognized from Ba and Mo analyses [40]). Consequently, we may regard S.S. material as one end member. As tempting as it is to label the grain B2-05 as the second end-member, we do not make this claim, but argue that B2-05 is the 'purest' grain measured in that study, displaying an isotopic composition most representative of this as-of-yet-unknown second end-member, which we take to be the actual stellar source of the SiC-X grains. Thus, the compositions of SiC-X grains do not represent *pure* nucleosynthetic signatures from stars but are best thought of as *mixtures* of an unknown exotic nucleosynthetic component from stars—which we denote SiC-X$_{EM}$ (EM: end-member)—*with* homogenized stardust of S.S. composition, where B2-05 is the cleanest stellar dust grain least diluted by this solar component. The precise, or rather the upper/lower limits, on the isotopic compositions of the hypothesized stellar source of SiC-X grains, SiC-X$_{EM}$, are constrained using the isotopic compositions of B2-05, recalling from isotope geochemistry that *in three-isotope space a mixture (R3) of any two components (R1 and R2) must fall on a line connecting R1 and R2 (c.f. parallelogram rule for vector addition in linear algebra)* [96]. From Figure 2 it is apparent that the nucleosynthetic end member SiC-X$_{EM}$ must fall on the respective mixing lines (i.e., linear regression lines) restricted to a subset of values laying on one side of B2-05, diametrically opposite the solar end member, such that the two end members (S.S. and SiC-X$_{EM}$) enclose the range of isotopic compositions displayed in these grains—see Figure 2, Equations (5) and (6) (where X = {Mo: $i$ = 92, 94, 95, 96, 98, 100 for $k$ = 97; Zr: $i$ = 91, 92, 94, 96 for $k$ = 90; Ru: $i$ = 96, 98, 99, 100, 102, 104 for $k$ = 101}).

$$^{i}X/^{k}X_{B205} \leq (\geq)\ ^{i}X/^{k}X_{SiC-X} \leq (\geq)\ ^{i}X/^{k}X_{SS} \quad (5)$$

$$^{i}X/^{k}X_{SiC-EM} \leq (\geq)\ ^{i}X/^{k}X_{B205} \quad (6)$$

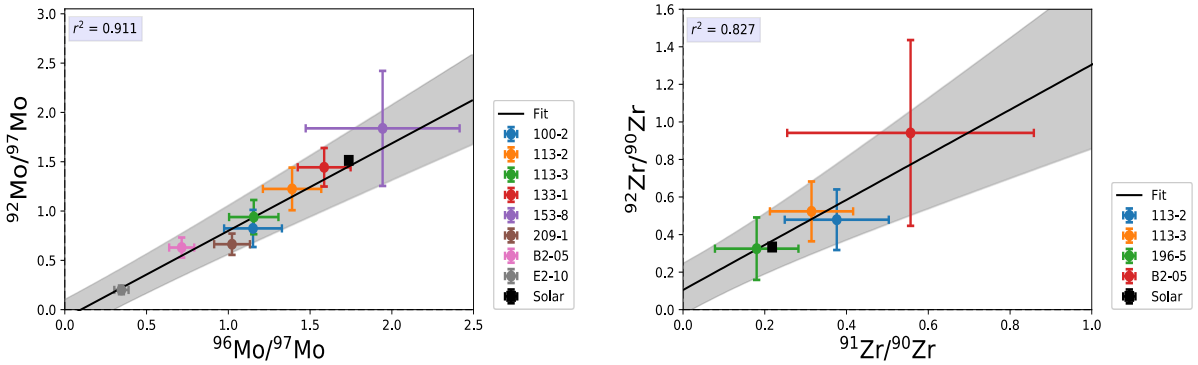



**Figure 2.** Molybdenum and Zr three-isotope plots for SiC-X grain data (2σ uncertainties) from [34]. Solar composition is included for reference purposes. Also shown are the 2D linear regression fits to the data (solid line), the associated 2σ errorband (shaded area) and quality of fit ($r^2$). Corresponding graphs for Ru not shown as there are only two SiC-X measurements, rendering a linear fit trivial. For completeness we also show the grain E2-10 for Mo (which was explored in the original analysis of [34] owing to the similar Mo isotope compositions of E2-10 and SiC-X grains) but exclude it from the fit. Regardless, the grain E2-10 falls on the mixing line.

From these considerations and the isotope data (together with their measurement uncertainties) from [34] we derive expressions for Zr, Mo and Ru that must be satisfied by the source of SiC-X grains (see column 2 in Table 1). Overall, we derive six isotopic inequalities for Mo (for the six isotope ratios: $^{i}$Mo/$^{97}$Mo; $i$ = 92, 94, 95, 96, 98, 100), four for Zr (four isotope ratios: $^{i}$Zr/$^{90}$Zr; $i$ = 91, 92, 94, 96), and six for Ru (six isotope ratios: $^{i}$Ru/$^{101}$Ru; $i$ = 96, 98, 99, 100, 102, 104), yielding a total of 16 expressions to constrain the stellar source of SiC-X grains. In the following section we compare these isotope ratio limits with stellar yields from leading nucleosynthesis models across diverse stellar sources to identify, and possibly constrain, the source of SiC-X grains.

## 6. The Nucleosynthetic Source of SiC-X Grains

We now explore various nucleosynthetic scenarios, ranging from new and updated classical models (s-, r-, p-process), the neutron-burst model, and our neutrino-driven wind model as possible candidates for the exotic SiC-X grain end-member (SiC-X$_{EM}$). Table 1 (column 2) displays the newly derived experimental limits on $^{i}$Mo/$^{k}$Mo, $^{i}$Zr/$^{k}$Zr, and $^{i}$Ru/$^{k}$Ru for SiC-X$_{EM}$ as determined by the methods described in Section 5.2. For Zr and Mo, these limits take into account the experimental uncertainties (2$\sigma$) on the composition of grain B2-05. In the case of Ru, the measurement uncertainties on B2-05 are too large to offer a reliable interpretation, so as a preliminary analysis we neglect the uncertainties and take the central value of the Ru isotope measurement of B2-05 at face value. Isotope ratios for select stellar models from each of the above mentioned scenarios are shown in the subsequent columns of Table 1. For each of the models in Table 1, we generate mixing lines in the relevant three-isotope space to illustrate the effect of mixing material from the corresponding stellar source with S.S., and overlay the SiC-X grain data to help visualize a match for SiC-X$_{EM}$ and the best fit to SiC-X grains in general.

### *6.1. s-Process*

The s-process yields in our mass range of interest are very sensitive to branching's (e.g., at $^{85}$Kr, $^{86}$Rb, $^{95}$Zr) and uncertainties on the corresponding (n,$\gamma$) reaction cross-sections, ultimately resulting in a spread of isotopic yields dependent upon ambient neutron densities, especially for Zr (for details see [97]). We focus primarily on s-process yields from the model of [98], which builds on the classic study of s-process nucleosynthesis in low mass AGB stars by [99], as our baseline or prototypical s-process model. To account for the potential spread in the theoretical isotope yields, owing to uncertain physical stellar conditions, we also explored the pulse-by-pulse (i.e., third dredge up, TDU) surface isotopic compositions—as opposed to final envelope compositions—for a range of initial mass progenitor stars, at different metallicities and $^{13}$C pocket efficiencies, for newly updated revisions of the same study by [98] that incorporate a more extensive nuclear reaction network and improved neutron-capture rates (in priv. comm. with S. Bisterzo and R. Gallino; Zr results published in [100]). These models are typically characterized by a distinct absence of $^{92}$Mo, and high $^{96}$Mo/$^{97}$Mo and $^{98}$Mo/$^{97}$Mo values relative to SiC-X grains, ruling out the s-process as the source of SiC-X grains. Quantitatively similar results are obtained for independent s-process models from (a) single stars over a similar if not more extensive parameter grid search (e.g., F.R.U.I.T.Y [101,102] and NuGrid [103,104]) as well as (b) galactic chemical evolution models (e.g., [26,105]). Figure 2 highlights the overall discrepancy between theory and data for Mo isotopes. Furthermore, the characteristic underproduction of $^{96}$Zr (usually requiring the $^{22}$Ne($\alpha$,n)$^{25}$Mg neutron source in such environments) and the absence of the p-isotopes $^{96,98}$Ru in s-process models necessitate that we look elsewhere to explain the anomalous isotopic signatures of SiC-X grains.

**Table 1.** Mo, Zr and Ru isotope compositions of the SiC-X end-member and various nucleosynthetic processes.

| | SiC-X End-Member Limit [a] | This Work [b] | n-Burst [c] | s-Process [d] | r-Process [e] | p-Process [f] |
|---|---|---|---|---|---|---|
| *[i]Mo/[k]Mo:* | | | | | | |
| $^{92}$Mo/$^{97}$Mo | ≤0.528 | $2.74 \times 10^{-3}$ | $1.43 \times 10^{-3}$ | 0 | 0 | ≈27 |
| $^{94}$Mo/$^{97}$Mo | ≤0.238 | $1.73 \times 10^{-3}$ | $3.28 \times 10^{-3}$ | 0.013 | 0 | ≈18 |
| $^{95}$Mo/$^{97}$Mo | ≈1.649 | 2.321 | 1.540 | 1.801 | 1.382 | ≈5 |
| $^{96}$Mo/$^{97}$Mo | ≤0.638 | $6.69 \times 10^{-5}$ | 0.010 | 3.27 | 0 | ≈4 |
| $^{98}$Mo/$^{97}$Mo | ≤1.133 | 1.654 | 0.379 | 3.28 | 1.247 | ≈4 |
| $^{100}$Mo/$^{97}$Mo | ≤0.390 | 0.637 | 0.095 | 0.072 | 2.683 | ≈2 |
| $^{92}$Mo/$^{94}$Mo | ≥2.578 | 1.587 | 0.437 | 0 | 0 | 1.527 |
| *[i]Zr/[90]Zr:* | | | | | | |
| $^{91}$Zr/$^{90}$Zr | ≥0.255 | 0.085 (0.193) [g] | 0.459 | 0.272 | 0 | 0.013 |
| $^{92}$Zr/$^{90}$Zr | ≥0.447 | 0.288 (0.700) [g] | 0.680 | 0.395 | 0 | 0.050 |
| $^{94}$Zr/$^{90}$Zr | ≥0.518 | 0.338 (0.844) [g] | 0.537 | 0.500 | 0 | 0.043 |
| $^{96}$Zr/$^{90}$Zr | ≥0.379 | 0.087 (0.298) [g] | 0.612 | 0.033 | 0.174 | 0.138 |
| *[i]Ru/[101]Ru:* | | | | | | |
| $^{96}$Ru/$^{101}$Ru | ≥0.935 | $3.86 \times 10^{-5}$ | $3.70 \times 10^{-9}$ | 0 | 0 | ≈135 |
| $^{98}$Ru/$^{101}$Ru | ≥0.177 | $2.76 \times 10^{-7}$ | $5.72 \times 10^{-7}$ | 0 | 0 | ≈62 |
| $^{99}$Ru/$^{101}$Ru | ≥1.141 | 0.184 | 0.473 | 1.398 | 0.607 | ≈13 |
| $^{100}$Ru/$^{101}$Ru | ≤0.338 | $5.76 \times 10^{-8}$ | $1.42 \times 10^{-3}$ | 4.576 | 0 | ≈16 |
| $^{102}$Ru/$^{101}$Ru | ≥2.755 | 4.489 | 10.20 | 5.223 | 1.123 | ≈1 |
| $^{104}$Ru/$^{101}$Ru | ≥2.883 | 0.542 | 7.41 | 0.152 | 1.294 | ≈7 |

[a] Upper/lower bounds on SiC-X end member (SiC-$X_{EM}$) compositions inferred using Equations (5) and (6). [b] Best case scenario for HEW nucleosynthesis occurs at $Y_e$ = 0.45, $S_{cum}$ = 94 (for Mo). [c] n-burst yields from [42], as reported in [40]. [d] s-process yields from [98]. [e] r-process yields calculated using r-residual method based on s-process yields from [98]. [f] p-process yields from [27]. [g] Yields in parentheses obtained for optimizing the HEW models for the Zr SiC-X grain data fits, which occur for $Y_e$ = 0.43, $S_{cum}$ = 76.

### 6.2. r-Process

The r-residual method, whereby the s-process contribution is subtracted from the S.S. composition, is used to calculate r-process yields. In its simplest formulation, nucleosynthetic contributions from additional sources (e.g., weak s-, weak r-, i-process) are ignored. Taking once again the s-process yields of [98] to represent s-process nucleosynthesis in AGB stars, the r-residual method yields an overproduction of $^{100}$Mo relative to SiC-X grains, whilst failing to provide a mechanism to synthesize the p-nuclei $^{92,94}$Mo already absent in the s-process models, nor sufficient quantities of $^{96}$Mo (shielded from the r-process production pathway by $^{96}$Zr). Aside from the r-residual method, more recent and seemingly promising candidates such as neutron-star mergers are equally unlikely as the synthesis of neutron-rich isotopes bypasses the lighter nuclei towards the Zr-Mo-Ru mass region.

### 6.3. p-Process

We showcase here the results of p-process models in Type Ia supernovae—the single degenerate case involving the thermonuclear explosion of a carbon-oxygen white dwarf pushed beyond the Chandrasekhar mass limit by accreting mass from its AGB companion. Travaglio et al. (2011) [27] assume an initial enhanced s-process seed distribution similar to the main s-process component in their model, arising from the earlier thermally pulsating AGB phase of the white dwarf and the later thermal pulses during the mass accretion phase. Consequently, [27] are able to not only reproduce S.S. p-nuclides (e.g., $^{92,94}$Mo, $^{96,98}$Ru) but also yield considerable s-only isotopes (e.g., $^{80}$Kr, $^{86}$Sr, $^{90}$Zr), as relics of the enhanced s-seed distribution, as well as some of the more neutron-rich isotopes (e.g., $^{96}$Zr) via the $^{22}$Ne(α,n)$^{25}$Mg reaction during the carbon-burning phase. The isotopic match with

presolar SiC-X grains is less satisfactory: (a) the normalization isotope $^{97}$Mo is the least abundant isotope in this model resulting in all $^{i}$Mo/$^{97}$Mo ratios > 1, which is not observed in SiC-X grains (see Table 1, Figure 3), (b) the two p-nuclides ($^{92,94}$Mo) are massively overproduced, relative to what is observed in the grains. Battino et al. (2020) [106] build up on the model presented in [27] using a more realistic seed distribution, obtaining globally similar results similar to [27], but ultimately discovering that $^{92,94}$Mo and $^{96}$Ru are not efficiently produced. We also considered intermediate- and high-mass single star systems in addition to the single-degenerate binary star system for the p-process, but these have their own limitations. Electron-capture supernovae of super AGB stars possessing a degenerate O-Ne-Mg core [25] synthesize large quantities of p-nuclei in the range Zn to Mo but are characterized by the marked absence (or serious underproduction) of neutron-rich isotopes $^{96}$Zr, $^{98,100}$Mo, $^{102,104}$Ru. The gamma-process in ccSNe has long since known to underproduce the dominant S.S. p-nuclides $^{92,94}$Mo and $^{96,98}$Ru, which is partly why modelers shifted their attention to other mechanisms/sites for the p-process (see, e.g., [107]). Recent galactic chemical evolution models factoring in the p-process from ccSNe also suffer from similar shortcomings [108], again making it hard to reconcile the isotopic signatures of SiC-X grains with the p-process.

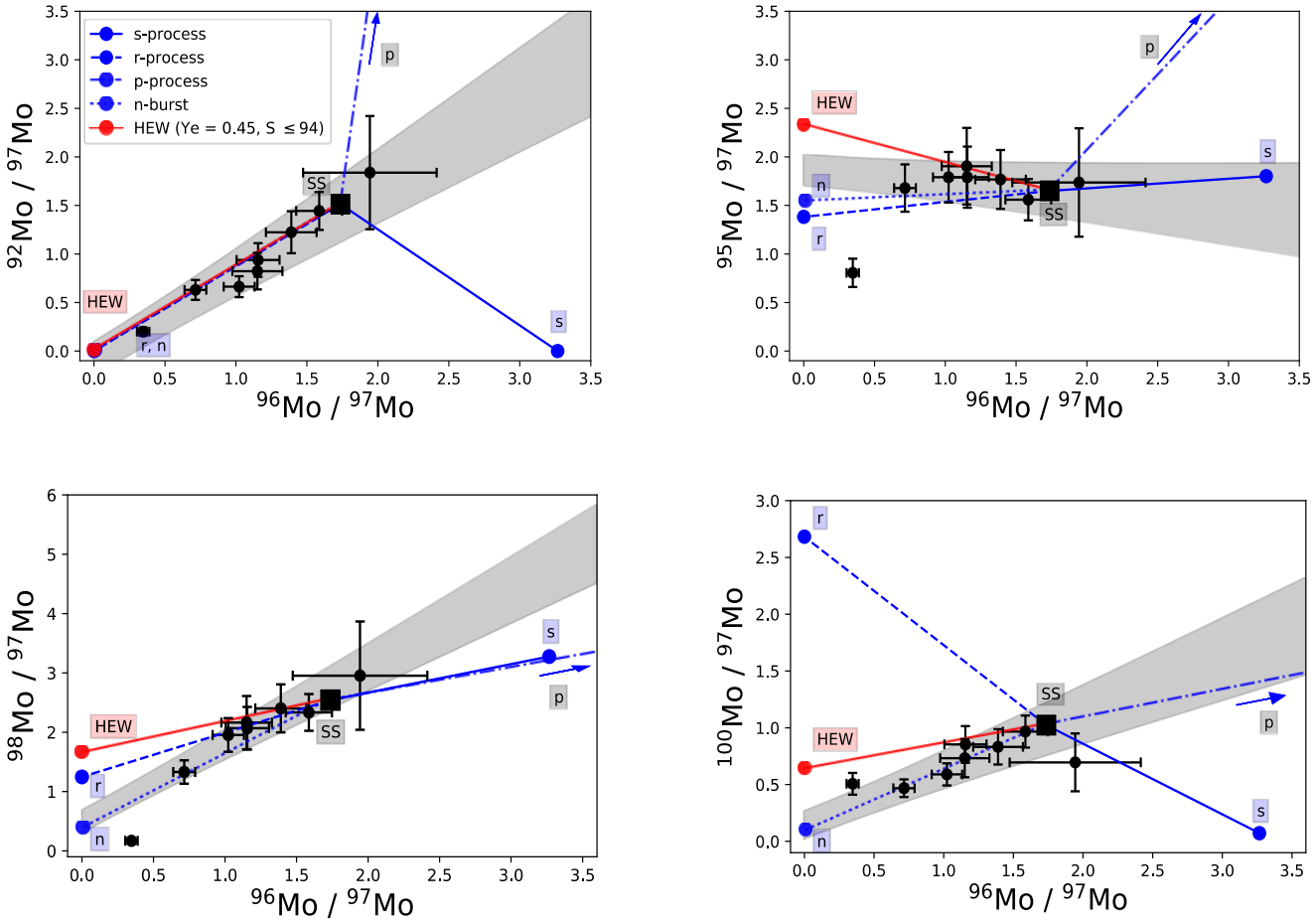



**Figure 3.** Molybdenum three-isotope plots for SiC-X grains overlaid with mixing lines for mixtures between various nucleosynthetic end-members and a S.S. component. Data uncertainties are 2σ. The error bands obtained from the 2D data fits (as in Figure 2) are displayed as shaded areas. Filled circles represent end-member compositions.

### *6.4. Neutron-Burst*

This is a generic term used to refer to a diverse class of processes characterized by a short burst of neutrons intermediate between an s- and an r-process, and is one of the

favoured go-to non-classical p-, s-, r-process models in the cosmochemistry community. The neutron-burst model rose to prominence after its initial success at providing an alternative solution to the heavy Xe isotope component (Xe-H) of the unusual Xe isotope compositions observed in presolar diamonds [109–111]. Thereafter, the neutron-burst model has been applied to a number of other cosmochemical scenarios (e.g., presence of the short-lived radionuclides $^{60}$Fe and $^{182}$Hf in the early S.S. [112]; isotopic anomalies in CAIs [113]; and as mentioned already, SiC-X grains [42]). Of the many neutron-burst models proposed (see for instance the models discussed in [40]) we focus on the scenario where the supernova shock wave traverses the He-rich shell of a massive star [41,42,111]. In this case, a pre-supernova weak s-process (duration typically $10^6$ years prior to explosion) acting on an initial solar distribution of nuclei is followed by irradiation from a neutrino-induced neutron-burst (duration: 10 s) during the supernova (shock) phase. We take here the updated yields—one year and one million years after the supernova explosion—provided to us by B. Meyer (in priv. comm. with W. Akram), based on [41,42]. Whereas [42] aim to reproduce the Mo isotopic composition of SiC-X grains using the same neutron-burst model parameters used by [41] to explain the Xe-H signature of presolar diamonds, we relax the constraints and take a more holistic approach to our analysis. The condensation of both types of grains (presolar diamond and SiC) in the same neutron-irradiated matter environment would be surprising (see [42]), and therefore we argue that it is not a requirement to explain both sets of observations using the same model parameters, albeit the same model. As already pointed out in [42] and demonstrated to some extent in Figure 3, the main characteristic pattern of SiC-X grains (excesses in $^{95}$Mo and $^{97}$Mo) are reproduced rather well by the neutron-burst model. The same model, however, synthesizes very little $^{92,94}$Mo (and $^{96,98}$Ru) leaving the grains to inherit much of the p-isotopes from the S.S. component. This result, combined with the 'secondary' nature of the neutron-burst, as it assumes an initial S.S. seed composition, warrants a look into alternative nucleosynthesis scenarios—in particular those capable of synthesizing the p-isotopes through means of a primary process and in more respectable quantities.

### *6.5. Neutrino-Driven Wind Component*

We present a more detailed and refined analysis of preliminary results published by our earlier investigations [31]. As mentioned in Section 4 we begin our exploration of the parameter space at $Y_e$ = 0.45, where the onset of p-isotopes (of Mo and Ru) is observed, largely focusing on $Y_e$ = 0.45, 0.47, 0.49—as already indicated by [31]. We explore the entire range of entropies from S = 10 $k_B$/baryon up to $\approx$ 270 $k_B$/baryon, computing isotopic yields for cumulative entropies ($S_{cum}$), with bin sizes of 4 $k_B$/baryon: setting $S_0$ = 10 we have $10 < S_1 \leq 14$, $10 < S_2 \leq 18$, ... , $10 < S_{64} \leq 270$ (Figure 1, right panel). For each of these cumulative entropy ranges we calculate the cumulative isotope ratios, which we take as the neutrino-driven wind end-member, and mix with the solar composition to obtain mixing lines. For all combinations of $Y_e$ and $S_{cum}$ explored, the best fit between the data (excluding grain E2-10) and mixing lines was obtained at $Y_e$ = 0.45 for $S_{cum} \approx 94$ $k_B$/baryon. Table 1 (column 3) displays the corresponding Mo, Zr and Ru isotope ratios obtained under these conditions of the neutrino-driven wind model. Surprisingly, our 'primary' nucleosynthesis model, which produces p-isotopes in greater quantities than the neutron-burst model, achieves similar $^{92}$Mo/$^{97}$Mo and $^{94}$Mo/$^{97}$Mo values as the neutron-burst model, such that both models satisfy the requirements for the SiC-X$_{EM}$ (for the p-isotopes at least). It is interesting to note that the SiC-X$_{EM}$ $^{95}$Mo/$^{97}$Mo value of 1.65 comes close to the S.S. value of 1.66. This is the likely reason why the neutron-burst model gives the better agreement ($^{95}$Mo/$^{97}$Mo = 1.54) than our best-fit neutrino-driven wind model ($^{95}$Mo/$^{97}$Mo = 2.32), as it assumes an initial S.S. composition for isotopes whereas our neutrino-driven wind model makes no such assumptions. Although $^{96}$Mo is underproduced in our model ($^{96}$Mo/$^{97}$Mo $\approx 7 \times 10^{-5}$), the $^{96}$Mo/$^{97}$Mo value still satisfies the SiC-X$_{EM}$ requirement ($^{96}$Mo/$^{97}$Mo $\leq$ 0.638). The heavier isotopes normalized to $^{97}$Mo ($^{98}$Mo/$^{97}$Mo and $^{100}$Mo/$^{97}$Mo) fall within a factor of two of the corresponding SiC-X$_{EM}$

values. A similar analysis optimizing the neutrino-driven wind mixing lines to the SiC-X data for Zr isotopes yields a best fit at slightly different, but still comparable conditions: lower electron fractions ($Y_e$ = 0.43) and entropies ($S_{cum}$ = 76 $k_B$/baryon)—see Table 1 (column 3). Under these $Y_e$-$S$ conditions, our neutrino-driven wind model reproduces the required SiC-$X_{EM}$ Zr isotope compositions within a factor of 2. The analysis for Ru is more tantalizing owing to the sparsity of available Ru isotope measurements for SiC-X grains and the relatively large measurement uncertainties associated with them. A preliminary analysis reveals that the best neutrino-driven wind model fits to what little Ru SiC-X grain data we have will require higher electron fractions and entropies ($Y_e \approx 0.47$, $S_{cum} \approx 120\ k_B$/baryon). In all cases (Zr, Mo and Ru) it is evident that the low-S, CP component of the neutrino-driven wind will (a) co-produce all stable p-, s-, and r-isotopes of Zr, Mo and Ru in respectable quantities and (b) reproduce the Zr, Mo (and Ru) isotope signatures of SiC-X grains, across a limited $Y_e$ band, confining the nucleosynthetic source region of SiC-X grains to a narrow and consistent set of astrophysical conditions within the neutrino-driven wind of ccSNe.

## 7. Conclusions

In this paper we presented a continuation of our exploration into the synthesis of the light trans-Fe elements within the framework of a neutrino-driven wind arising from the newly born proto-neutron star in ccSNe. We highlighted a few key improvements to our earlier studies, including the importance of using a unified approach to nuclear physics in our nucleosynthesis calculations. Also re-emphasized were a few key theoretical results from our early investigations [31]: the parameterization of our model in terms of just $S$, $Y_e$ and $V_{exp}$, and the delineation of distinct nucleosynthesis modes (charged-particle and neutron-captures) at different $Y_e$-$S$ combinations. Following on from the initial success of our model in explaining *elemental* abundances in UMPs, we shifted our attention to *isotopic* compositions within early S.S. materials. We focused on the low-S ($S \leq$ 100–150 $k_B$/baryon), charged-particle component of our neutrino-driven wind scenario and confirm that for moderate electron abundances ($0.44 \leq Y_e \leq 0.49$) our model is able to synthesize p-, s-, and r-isotopes in the light trans-Fe mass region between Zn (Z = 30) and Ru (Z = 44) in considerable quantities. We also stress the 'primary' nature of our model whereby no requirement is invoked for the initial seed distribution of nuclei prior to nucleosynthesis, i.e., we do not assume a starting S.S. composition with p-nuclei already present.

We limited our analysis to the (re-)analysis of the highly anomalous Zr, Mo and Ru isotope compositions of the rare subset of SiC grains denoted type X, SiC-X grains, which have so far evaded a classical p, s, r-process origin. The key results of our cosmochemical analysis utilizing three-isotope plots and mixing lines are as follows: (1) A review of new and updated p-, s-, and r-process models reveal that we are in no better a position than the initial studies that indicated the failure of the classical p-, s-, r-process to account for the anomalous isotopic compositions of these grains. The neutron-burst model remains a plausible option but we reiterate that it is strongly dependent upon the initial distribution of seed nuclei and peak temperature of the burst. (2) All p-, s-, and r-process isotopes of Zr, Mo and Ru are co-produced in the low-S component, thereby alleviating the dependence of the neutron-capture processes (e.g., weak-r) in this mass region, leading in particular to a re-evaluation of the initial S.S. abundance estimates based on the classical p-, s-, r-decomposition. (3) The anomalous Zr, Mo (and within the uncertainties, Ru) isotope compositions of SiC-X grains are reproduced well under a narrow and well-confined band of $S$-$Y_e$ parameter combinations, reflecting a consistent and realistic set of astrophysical conditions within the low-$S$, CP component of the neutrino-driven wind scenario in ccSNe. (4) The grains do not possess 'clean' signatures of the neutrino-driven wind in ccSNe but are admixtures of select neutrino-driven wind material mixed with S.S. material, with grain B2-05 the 'purest' grain identified to date, having preserved as much of the initial neutrino-driven wind signature. Upon correction of this S.S. contribution one may argue that these SiC-X grains are possibly the only 'clean' signature of a standard ccSN neutrino-driven wind

scenario identified so far—and do not require additional r-process components from other explosive scenarios such as magneto-rotational SN-jets or neutron-star merger events.

**Author Contributions:** W.A.: conceptualization, methodology, writing, formal analysis, investigation. O.H.: conceptualization, methodology, formal analysis, investigation. B.P.: formal analysis. K.-L.K.: conceptualization, methodology, writing, formal analysis, investigation. All authors have read and agreed to the published version of the manuscript.

**Funding:** This research received no external funding.

**Institutional Review Board Statement:** Not Applicable.

**Informed Consent Statement:** Not Applicable.

**Acknowledgments:** The authors wish to thank: K. Farouqi for the initial development of the models and parameter studies, without which this work would not be possible; U. Ott for his early involvement with this work; B. Meyer for useful insight and permission to use his neutron-burst models; and M. Busso and R. Gallino for sharing their knowledge of s-process nucleosynthesis with us over the years as well as providing access to their latest s-process models.

**Conflicts of Interest:** The authors declare no conflict of interest.

## References

1. Merrill, P.W. Spectroscopic observations of stars of class. *Astrophys. J.* **1952**, *116*, 22–26. [CrossRef]
2. Goldschmidt, V.M. *Geochemische Verteilungsgesetze der Elemente*; Skrifter Norske Videnskaps-Acd: Oslo, Norway, 1926.
3. Suess, H.E.; Urey, H.C. Abundances of the elements. *Rev. Mod. Phys.* **1956**, *28*, 53–74. [CrossRef]
4. Burbidge, E.M.; Burbidge, G.R.; Fowler, W.A.; Hoyle, F. Synthesis of the elements in stars. *Rev. Mod. Phys.* **1957**, *29*, 547–650. [CrossRef]
5. Cameron, A.G.W. *Stellar Evolution, Nuclear Astrophysics, and Nucleogenesis*; Chalk River Report 1957, CRL-41; Atomic Energy of Canada Ltd.: Chalk River, ON, Canada, 1957.
6. Arnould, M. Possibility of synthesis of proton-rich nuclei in highly evolved stars II. *Astron. Astrophys.* **1976**, *46*, 117–125.
7. Woosley, S.E.; Howard, W.M. The p-process in supernovae. *Astrophys. J.* **1978**, *36*, 285–304. [CrossRef]
8. Clayton, D.D. *Principles of Stellar Evolution and Nucleosynthesis*; McGraw Hill: New York, NY, USA, 1968.
9. Käppeler, F.; Beer, H.; Wisshak, K. S-process nucleosynthesis-nuclear physics and the classical model. *Rep. Prog. Physics.* **1989**, *52*, 945. [CrossRef]
10. Seeger, P.A.; Fowler, W.A.; Clayton, D.D. Nucleosynthesis of heavy elements by neutron capture. *Astrophys. J.* **1965**, *11*, 121–166. [CrossRef]
11. Hillebrandt, W. The rapid neutron-capture process and the synthesis of heavy and neutron-rich elements. *Space Sci. Rev.* **1978**, *21*, 639–702. [CrossRef]
12. Cowan, J.J.; Thielemann, F.-K.; Truran, J.W. The r-process and nucleochronology. *Phys. Rep.* **1991**, *208*, 267–394. [CrossRef]
13. Roederer, I.U.; Cowan, J.J.; Karakas, A.I.; Kratz, K.-L.; Lugaro, M.; Simmerer, J.; Farouqi, K.; Sneden, C. The ubiquity of the rapid neutron-capture process. *Astrophys. J.* **2010**, *724*, 975–993. [CrossRef]
14. Hill, V.; Christlieb, N.; Beers, T.C.; Barklem, P.S.; Kratz, K.-L.; Nordström, B.; Pfeiffer, B.; Farouqi, K. The Hamburg/ESO r-process enhanced star survey (HERES). *Astron. Astrophys.* **2017**, *607*, A91.
15. Hansen, T.T.; Holmbeck, E.M.; Beers, T.C.; Placco, V.M.; Roederer, I.U.; Frebel, A.; Sakari, C.M.; Simon, J.D.; Thompson, I.B. The r-process alliance: First release from the southern search for r-process-enriched stars in the galactic halo. *Astrophys. J.* **2018**, *858*, 92–108. [CrossRef]
16. Frebel, A.; Beers, T.C. The formation of the heaviest elements. *Phys. Today* **2018**, *71*, 30–37. [CrossRef]
17. Kratz, K.-L.; Bitouzet, J.-P.; Thielemann, F.-K.; Möller, P.; Pfeiffer, B. Isotopic r-process abundances and nuclear structure far from stability: Implications for the r-process mechanism. *Astrophys. J.* **1993**, *403*, 216–238. [CrossRef]
18. Kratz, K.-L.; Farouqi, K.; Pfeiffer, B.; Truran, J.W.; Sneded, C.; Cowan, J.J. Explorations of the r-process: Comparisons between calculations and observations of low-metallicity stars. *Astrophys. J.* **2007**, *662*, 39–52. [CrossRef]
19. Kratz, K.-L.; Farouqi, K.; Möller, P. A high-entropy-wind r-process study based on nuclear-structure quantities from the new finite-range droplet model FRDM(2012). *Astrophys. J.* **2014**, *792*, 6–12. [CrossRef]
20. Hoffman, R.D.; Woosley, S.E.; Fuller, G.M.; Meyer, B.S. Production of the light p-process nuclei in neutrino-driven winds. *Astrophys. J.* **1996**, *460*, 478–488. [CrossRef]
21. Hoffman, R.D.; Woosley, S.E.; Qian, Y.-Z. Nucleosynthesis in neutrino-driven winds II-implications for heavy element synthesis. *Astrophys. J.* **1997**, *482*, 951–962. [CrossRef]
22. Hoffman, R.D.; Müller, B.; Janka, H.-T. Nucleosynthesis in O-Ne-Mg supernovae. *Astrophys. J.* **2008**, *676*, L127–L130. [CrossRef]
23. Rauscher, T.; Heger, A.; Hoffman, R.D.; Woosley, S.E. Nucleosynthesis in massive stars with improved nuclear and stellar physics. *Astrophys. J.* **2002**, *576*, 323–348. [CrossRef]

24. Pignatari, M.; Gallino, R.; Meynet, G.; Hirschi, R.; Herwig, F.; Wiescher, M. The s-process in massive stars at low metallicity: The effect of primary 14N from fast rotating stars. *Astrophys. J.* **2008**, *687*, L95–L98. [CrossRef]
25. Wanajo, S.; Nomoto, K.; Janka, H.-T.; Kitaura, F.S.; Müller, B. Nucleosynthesis in electron capture supernovae of asymptotic giant branch stars. *Astrophys. J.* **2009**, *695*, 208–220. [CrossRef]
26. Travaglio, C.; Gallino, R.; Arnone, E.; Cowan, J.; Jordan, F.; Sneden, C. Galactic evolution of Sr, Y, and Zr: A multiplicity of nucleosynthetic processes. *Astrophys. J.* **2004**, *601*, 864–884. [CrossRef]
27. Travaglio, C.; Röpke, F.K.; Gallino, R.; Hillebrandt, W. Type Ia supernovae as sites of the p-process: Two-dimensional models coupled to nucleosynthesis. *Astrophys. J.* **2011**, *793*, 93–111. [CrossRef]
28. Travaglio, C.; Gallino, R.; Rauscher, T.; Röpke, F.K.; Hillebrandt, W. Testing the role of SNe Ia for galactic chemical evolution of p-nuclei with two-dimensional models and with s-process seeds at different metallicities. *Astrophys. J.* **2015**, *799*, 54–68. [CrossRef]
29. Farouqi, K.; Kratz, K.-L.; Cowan, J.J.; Mashonkina, L.I.; Pfeiffer, B.; Sneden, C.; Thielemann, F.-K.; Truran, J.W. Nucleosynthesis modes in the high-entropy-wind scenario of type II supernovae. In *AIP Conference Proceedings*; O'Shea, B.W., Heger, A., Abel, T., Eds.; First Stars III; AIP Publishing: Long Island, NY, USA, 2008; Volume 990, pp. 309–314.
30. Farouqi, K.; Kratz, K.-L.; Mashonkina, L.I.; Pfeiffer, B.; Cowan, J.J.; Thielemann, F.-K.; Truran, J.W. Nucleosynthesis modes in the high-entropy wind of type II supernovae: Comparison of calculations with halo-star observations. *Astrophys. J.* **2009**, *694*, L49–L53. [CrossRef]
31. Farouqi, K.; Kratz, K.-L.; Pfeiffer, B. Co-production of light p-, s- and r-process isotopes in the high-entropy wind of type II supernovae. *Publ. Astron. Soc. Aust.* **2009**, *26*, 194–202. [CrossRef]
32. Farouqi, K.; Kratz, K.-L.; Pfeiffer, B.; Rauscher, T.; Thielemann, F.-K.; Truran, J.W. Charged-particle and neutron-capture processes in the high-entropy wind of core-collapse supernovae. *Astrophys. J.* **2010**, *712*, 1359–1377. [CrossRef]
33. Pellin, M.J.; Davis, A.M.; Calaway, W.F.; Lewis, R.S.; Clayton, R.N. Zr and Mo isotopic constraints on the origins of unusual types of presolar SiC grains. In Proceedings of the 31st Lunar and Planetary Science Conference, Houston, TX, USA, 13–17 March 2000; Available online: https://www.lpi.usra.edu/lpi/meteorites/lpsc31abs.html (accessed on 1 July 2022).
34. Pellin, M.J.; Savina, M.R.; Calaway, W.F.; Tripa, C.E.; Barzyk, J.G.; Davis, A.M.; Gyngard, F.; Amari, S.; Zinner, E.; Lewis, R.S.; et al. Heavy metal isotopic anomalies in supernovae presolar grains. In Proceedings of the Lunar and Planetary Science Conference Proceedings, XXXVII 2006, #2041, League City, TX, USA, 13–17 March 2006.
35. Birck, J.-L. An overview of isotopic anomalies in extraterrestrial materials and their nucleosynthetic heritage. *Rev. Mineral. Geochem.* **2004**, *55*, 25–64. [CrossRef]
36. Akram, W.; Schönbächler, M.; Sprung, P.; Vogel, N. Zirconium-hafnium isotope evidence from meteorites for the decoupled synthesis of light and heavy neutron-rich nuclei. *Astrophys. J.* **2013**, *777*, 169–180. [CrossRef]
37. Ott, U. Isotope variations in the solar system: Supernova fingerprints. In *Handbook of Supernovae*; Alsabi, A.W., Murdin, P., Eds.; Springer: Berlin/Heidelberg, Germany, 2016.
38. Zinner, E. Presolar Grains. In *Treatise on Geochemistry*, 2nd ed.; Holland, H.D., Turekian, K.K., Eds.; Elsevier: Amsterdam, The Netherlands, 2014; pp. 181–213.
39. Clayton, D.D. *Handbook of Isotopes in the Cosmos*; Cambridge University Press: Cambridge, UK, 2003.
40. Marhas, K.K.; Hoppe, P.; Ott, U. NanoSIMS studies of Ba isotopic compositions in single presolar silicon carbon grains from AGB stars and supernovae. *MAPS* **2007**, *42*, 1077–1101.
41. Howard, W.M.; Meyer, B.S.; Clayton, D.D. Heavy-element abundances from a neutron burst that produces Xe-H. *Meteoritics* **1992**, *27*, 404–412. [CrossRef]
42. Meyer, B.S.; Clayton, D.D.; The, L.S. Molybdenum and zirconium isotopes from a supernova neutron burst. *Astrophys. J.* **2000**, *540*, L49–L52. [CrossRef]
43. Hallmann, O.; Farouqi, K.; Kratz, K.-L.; Ott, U. Origin of Anomalous Zr, Mo and Ru Abundances in SiC X-grains: Indications of a Primary Charged-Particle Process. 76th Annual Meteoritical Society Meeting 2013, #5082. Available online: https://www.hou.usra.edu/meetings/metsoc2013/pdf/5082.pdf (accessed on 12 December 2021).
44. Kratz, K.L.; Akram, W.; Farouqi, K.; Hallmann, O. Production of light trans-Fe elements in core collapse supernovae: Implications from presolar SiC-X grains. *AIP Conf. Proc.* **2019**, *2076*, 030002.
45. Thielemann, F.-K.; Ken'Ichi, N.; Masa-Aki, H. Core-collapse supernova and their ejecta. *Astrophys. J.* **1996**, *460*, 408–436. [CrossRef]
46. Fröhlich, C.; Martínez-Pinedo, G.; Liebendörfer, M.; Thielemann, F.-K.; Bravo, E.; Hix, W.R.; Langanke, K.; Zinner, N.T. Neutrino-induced nucleosynthesis of A > 64 nuclei: The nu-p process. *Phys. Rev. Lett.* **2006**, *96*, 145502. [CrossRef] [PubMed]
47. Freiburghaus, C.; Rembges, J.-F.; Rauscher, T.; Kolbe, E.; Thielemann, F.-K.; Kratz, K.-L.; Pfeiffer, B.; Cowan, J.J. The astrophysical r-process: A comparison of calculations following adiabatic expansion with classical calculations based on neutron densities and temperatures. *Astrophys. J.* **1999**, *516*, 381–398. [CrossRef]
48. Meyer, B.S.; Matthews, G.J.; Howard, W.M.; Woosley, S.E.; Hoffman, R.D. R-process nucleosynthesis in the high-entropy supernova bubble. *Astrophys. J.* **1992**, *399*, 656–664. [CrossRef]
49. Kratz, K.-L.; Thielemann, F.-K.; Willebrandt, W.; Möller, P.; Harms, V.; Wohr, A.; Truran, J.W. Constraints on r-process conditions from beta-decay properties far off stability and r-abundances. *J. Phys. G* **1988**, *14*, S331. [CrossRef]
50. Möller, P.; Nix, J.R. Calculation of fission barriers with the droplet model and folded Yukawa single-particle model. *Nucl. Phys. A* **1974**, *229*, 269–291. [CrossRef]

51. Möller, P.; Nix, J.R. Atomic masses and nuclear ground-state deformations calculated with a new macroscopic-microscopic model. *At. Data Nucl. Data Tables* **1981**, *26*, 165–196. [CrossRef]
52. Krumlinde, J.; Möller, P. Calculation of Gamow-Teller beta-strength functions in the rubidium region in the RPA approximation with Nilsson-model wave functions. *Nucl. Phys. A* **1984**, *417*, 419–446. [CrossRef]
53. Möller, P.; Randrup, J. New developments in the calculation of beta-strength functions. *Nucl. Phys. A* **1990**, *514*, 1–48. [CrossRef]
54. Möller, P.; Nix, J.R.; Myers, W.D.; Swiatecki, W.J. Nuclear ground-state masses and deformations. *At. Data Nucl. Data Tables* **1995**, *59*, 185–381. [CrossRef]
55. Möller, P.; Nix, J.R.; Kratz, K.-L. Nuclear properties for astrophysical and radioactive ion-beam applications. *At. Data Nucl. Data Tables* **1997**, *66*, 131–343. [CrossRef]
56. Möller, P.; Pfeiffer, B.; Kratz, K.-L. New calculations of gross beta-decay properties for astrophysical applications: Speeding up the classical r process. *Phys. Rev. C* **2003**, *67*, 055802. [CrossRef]
57. Takahashi, K. Application of the Gross theory of beta-decay to delayed neutron emissions. *Prog. Theor. Phys.* **1972**, *47*, 1500–1516. [CrossRef]
58. Kratz, K.L.; Ohm, H.; Schröder, A.; Gabelmann, H.; Ziegert, W.; Pfeiffer, B.; Jung, G.; Monnand, E.; Pinston, J.A.; Schussler, F.; et al. The beta-decay of 95Rb and 97Rb. *Z. Phys.* **1983**, *312*, 43–57. [CrossRef]
59. Raman, S.; Fogelberg, B.; Harvey, J.A.; Macklin, R.L.; Stelson, P.H.; Schröder, A.; Kratz, K.-L. Overlapping beta decay and resonance neutron spectroscopy of levels in 87Kr. *Phys. Rev. C* **1983**, *28*, 602. [CrossRef]
60. Eberth, J.; Meyer, R.A.; Sistemich, K. *Int. Workshop in Nuclear Structure in the Zirconium Region*; Springer: Berlin/Heidelberg, Germany, 1988.
61. Lhersonneau, G.; Pfeiffer, B.; Kratz, K.-L.; Enqvist, T.; Jauho, P.P.; Jokinen, A.; Kantele, J.; Leino, M.; Parmonen, J.M.; Penttilä, H.; et al. Evolution of deformation in the neutron-rich Zr region from excited intruder state to the ground state. *Phys. Rev. C* **1994**, *49*, 1379. [CrossRef]
62. Kratz, K.-L.; Gabelmann, H.; Pfeiffer, B.; Möller, P. Onset of deformation in neutron-rich krypton isotopes. *Z. Phys.* **1988**, *330*, 229–230. [CrossRef]
63. Lhersonneau, G.; Wöhr, A.; Pfeiffer, B.; Kratz, K.-L.; the ISOLDE Collaboration. First decay study of the very neutron-rich isotope 93Br. *Phys. Rev. C* **2001**, *63*, 034316. [CrossRef]
64. Pfeiffer, B.; Kratz, K.-L.; Möller, P. Status of delayed-neutron precursor data: Half-lives and neutron emission probabilities. Prog. *Nucl. Energy* **2002**, *41*, 39–69. [CrossRef]
65. Bergemann, U.C.; Diget, C.A.; Riisager, K.; Weissman, L.; Auböck, G.; Cederkäll, J.; Fraile, L.M.; Fynbo, H.O.U.; Gausemel, H.; Jeppensen, H.; et al. Beta-decay properties of the neutron-rich 94-99Kr and 142-147Xe isotopes. *Nucl. Phys. A* **2003**, *714*, 21–43. [CrossRef]
66. Kratz, K.-L.; Ziegert, W.; Hillebrandt, W.; Thielemann, F.-K. Determination of stellar neutron-capture rates for radioactive nuclei with the aid of beta-delayed neutron emission. *Astron. Astrophys.* **1983**, *125*, 381–387.
67. Kratz, K.-L. Relevance of beta-delayed neutron data for reactor, nuclear physics and astrophysics applications. In Exotic Nuclei and Nuclear/Particle Astrophysics V: From Nuclei to Stars. *AIP Conf. Proc.* **2014**, *1645*, 109–120.
68. Thielemann, F.-K.; Arnould, M.; Truran, J.W. *Advances in Nuclear Physics: Proceedings of the Second IAP Workshop, Paris, France*; Vangioni-Flam, E., Audouze, J., Casse, M., Chieze, J.-P., Tran Thanh Van, J., Eds.; Gif-sur-Yvette, France: Editions Frontières; EDP Sciences: Les Ulis, France, 1986; p. 525.
69. Rauscher, T.; Thielemann, F.-K.; Kratz, K.-L. The nuclear level density and the determination of thermonuclear rates for astrophysics. *Mem. Soc. Astron. Ital.* **1996**, *67*, 851. [CrossRef]
70. Rauscher, T.; Thielemann, F.-K.; Kratz, K.-L. Applicability of the Hauser-Feshbach approach for the determination of astrophysical reaction rates. *Nucl. Phys. A* **1997**, *621*, 331–334. [CrossRef]
71. Rauscher, T.; Thielemann, F.-K. Astrophysical reaction rates from statistical model calculations. *At. Data Nucl. Data Tables* **2000**, *75*, 1–351. [CrossRef]
72. Rauscher, T.; Thielemann, F.-K. Tables of nuclear cross sections and reaction rates. *At. Data Nucl. Data Tables* **2001**, *79*, 47–64. [CrossRef]
73. Oberhummer, H.; Staudt, G. *Nuclei in the Cosmos*; Springer: Berlin/Heidelberg, Germany, 1991; p. 29.
74. Kraussmann, E.; Balogh, W.; Oberhummer, H.; Rauscher, T.; Kratz, K.-L.; Ziegert, W. Direct neutron capture for magic-shell nuclei. *Phys. Rev. C* **1996**, *53*, 469. [CrossRef] [PubMed]
75. Rauscher, T.; Bieber, R.; Oberhummer, H.; Kratz, K.-L.; Dobaczewski, J.; Möller, P.; Sharma, M.M. Dependence of direct neutron capture on nuclear-structure models. *Phys. Rev. C* **1998**, *57*, 2031. [CrossRef]
76. Kratz, K.-L.; Böhmer, W.; Freiburghaus, C.; Möller, P.; Pfeiffer, B.; Rauscher, T.; Thielemann, F.-K. On the origin of the Ca-Ti-Cr isotopic anomalies in the inclusion EK-1-4-1 of the Allende-meteorite. *Mem. Della Soc. Astron. Ital.* **2001**, *72*, 453–466.
77. Nuh, F.M.; Slaughter, D.R.; Prussin, S.G.; Ohm, H.; Rudolph, W.; Kratz, K.-L. Delayed neutrons and high-energy gamma rays from decay of 87Br. *Nucl. Phys. A* **1977**, *293*, 410–424. [CrossRef]
78. Kratz, K.-L.; Rudolph, W.; Ohm, H.; Franz, H.; Zendel, M.; Herrmann, G.; Prussin, S.G.; Nuh, F.M.; Shihab-Elbin, A.A.; Slaughter, D.R.; et al. Investigation of beta strength functions by neutron and gamma-ray spectroscopy. *Nucl. Phys. A* **1979**, *317*, 335–362. [CrossRef]

79. Leist, B.; Ziegert, W.; Wiescher, M.; Kratz, K.-L.; Thielemann, F.-K. Neutron capture cross sections for neutron-rich isotopes. *Z. Phys.* **1985**, *322*, 531–532. [CrossRef]
80. Ewan, G.T.; Hoff, P.; Jonson, B.; Kratz, K.-L.; Larsson, P.O.; Nyman, G.; Ravn, H.L.; Ziegert, W. Intense mass-separated beams of halogens and beta-delayed neutron emission from heavy bromine isotopes. *Z. Phys.* **1984**, *318*, 309–314.
81. Kratz, K.L. Proc. Consultants' Meeting on Delayed Neutron Properties. Vienna, 1979. International Nuclear Data Committee, International Atomic Energy Agency (NDS)-107, 103. Available online: https://www-nds.iaea.org/publications/indc/indc-nds-0107/ (accessed on 1 July 2022).
82. Schröder, A.; Ohm, H.; Rudolph, W.; Sümmerer, K.; Kratz, K.-L.; Wünsch, K.D.; Jung, G.; Crançon, J.; Ristori, C. Spectroscopy of beta-delayed neutrons in coincidence with gamma-rays depopulating excited states in 93Sr. *Phys. Lett. B* **1980**, *90*, 57–60. [CrossRef]
83. Holmes, J.A.; Woosley, S.E.; William, A.; Fowler, B.A.; Zimmerman, B.A. Tables of thermonuclear-reaction-rate data for neutron-induced reactions on heavy nuclei. *At. Data Nucl. Data Tables* **1976**, *18*, 305–412. [CrossRef]
84. Porter, C.E.; Thomas, R.G. Fluctuations of nuclei reaction widths. *Phys. Rev.* **1956**, *104*, 483. [CrossRef]
85. Ohm, H.; Zendel, M.; Prussin, S.G.; Rudolph, W.; Schröder, A.; Kratz, K.-L.; Ristori, C.; Pinston, J.A.; Monnand, E.; Schussler, F.; et al. Beta-delayed neutrons and high-energy gamma-rays from decay of 137I. *Z. Phys.* **1980**, *296*, 23–33. [CrossRef]
86. Reynolds, J.H.; Turner, G. Rare gases in the chondrite Renazzo. *J. Geophys. Res.* **1964**, *69*, 3263–3281. [CrossRef]
87. Lewis, R.S.; Anders, E.; Draine, B.T. Properties, detectability and origin of interstellar diamonds in meteorites. *Nature* **1987**, *339*, 117–121. [CrossRef]
88. Bernatowicz, T.; Fraundorf, G.; Ming, T.; Anders, E.; Wopenka, B.; Zinner, E.; Fraundorf, P. Evidence for interstellar SiC in the Murray carbonaceous chondrite. *Nature* **1987**, *330*, 24–31. [CrossRef]
89. Tang, M.; Anders, E. Isotopic anomalies of Ne, Xe, and C in meteorites. II. Interstellar diamond and SiC: Carriers of exotic noble gases. *Geochim. Cosmochim. Acta* **1988**, *52*, 1235–1244.
90. Amari, S.; Anders, E.; Virag, A.; Zinner, E. Interstellar graphite in meteorites. *Nature* **1990**, *345*, 238–240. [CrossRef]
91. McSween, H.Y., Jr.; Huss, G.R. *Cosmochemistry*; Cambridge University Press: Cambridge, UK, 2010.
92. Amari, S.; Hoppe, P.; Zinner, E.; Lewis, R.S. Interstellar SiC with unusual isotopic compositions: Grains from a supernova? *Astrophys. J.* **1992**, *394*, L43–L46. [CrossRef]
93. Amari, S.; Lewis, R.S.; Anders, W. Interstellar grains in meteorites: I. isolation of SiC, graphite, and diamond; size distributions of SiC and graphite. *Geochim. Cosmochim. Acta* **1994**, *58*, 459–470. [CrossRef]
94. Davis, A.M.; Pellin, M.; Lewis, R.; Amari, S.; Clayton, R. Molybdenum and Zirconium Isotopic Compositions of Supernova Grains. 62nd Annual Meteoritical Society Meeting 1999, #5202. Available online: https://www.lpi.usra.edu/meetings/metsoc99/pdf/5202.pdf (accessed on 1 July 2022).
95. Savina, M.R.; Pellin, M.J.; Tripa, C.E.; Veryovkin, I.V.; Calaway, W.F.; Davis, A.M. Analyzing individual presolar grains with CHARISMA. *Geochim. Cosmochim. Acta* **2003**, *67*, 3215–3225. [CrossRef]
96. Allègre, C.J. *Isotope Geology*; Cambridge University Press: Cambridge, UK, 2008.
97. Lugaro, M.; Davis, A.M.; Gallino, R.; Pellin, M.J.; Straniero, O.; Käppeler, F. Isotopic compositions of strontium, zirconium, molybdenum, and barium in single presolar SiC grains and asymptotic giant branch stars. *Astrophys. J.* **2003**, *593*, 486–508. [CrossRef]
98. Bisterzo, S.; Gallino, R.; Straniero, O.; Cristallo, S.; Käppeler, F. The s-process in low metallicity stars-II. *Mon. Not. R. Astron. Soc.* **2011**, *418*, 284–319. [CrossRef]
99. Arlandini, C.; Käppeler, F.; Wisshak, K.; Gallino, R.; Lugaro, M.; Busso, M.; Straniero, O. Neutron capture in low-mass asymptotic giant branch stars: Cross sections and abundance signatures. *Astrophys. J.* **1999**, *525*, 886–900. [CrossRef]
100. Akram, W.; Schönbächler, M.; Bisterzo, S.; Gallino, R. Zirconium isotope evidence for the heterogeneous distribution of s-process materials in the solar system. *Geochim. Cosmochim. Acta* **2015**, *165*, 484–500. [CrossRef]
101. Cristallo, S.; Piersanti, L.; Straniero, O.; Gallino, R.; Domínguez, I.; Abia, C.; Rico, G.D.; Quintini, M.; Bisterzo, S. Evolution, nucleosynthesis, and yields of low-mass asymptotic giant branch stars at different metallicities II-the fruity database. *Astrophys. J.* **2011**, *197*, 17–38. [CrossRef]
102. Cristallo, S.; Piersanti, L.; Straniero, O. The FRUITY database on AGB stars: Past, present and future. *J. Phys. Config. Ser.* **2016**, *665*, 012019. [CrossRef]
103. Pignatari, M.; Herwig, F.; Hirschi, R.; Bennett, M.; Rockefeller, G.; Fryer, C.; Timmes, F.X.; Ritter, C.; Heger, A.; Jones, S.; et al. Nugrid stellar data set I. stellar yields from H to Bi for stars with metallicities Z = 0.02 and Z 0.01. *Astrophys. J.* **2016**, *225*, 24–49. [CrossRef]
104. Battino, U.; Tattersall, A.; Lederer-Woods, C.; Herwig, F.; Denissenkov, P.; Hirschi, R.; Trappitsch, R.; den Hartogh, J.W.; Pignatari, M. Nugrid stellar data set III. updated low-mass AGB models and s-process nucleosynthesis with metallicities Z = 0.01, Z = 0.02, and Z = 0.03. *Mon. Not. R. Astron. Soc.* **2019**, *489*, 1082–1098. [CrossRef]
105. Bisterzo, S.; Travaglio, C.; Gallino, R.; Wiescher, M.; Käppeler, F. Galactic chemical evolution and solar s-process abundances: Dependence on the 13C-pocket structure. *Astrophys. J.* **2014**, *787*, 787–800. [CrossRef]
106. Battino, U.; Pignatari, M.; Travaglio, C.; Lederer-Woods, C.; Denissenkov, P.; Herwig, F.; Thielemann, F.; Rauscher, T. Heavy elements nucleosynthesis on accreting white dwarfs: Building seeds for the p-process. *Mon. Not. R. Astron. Soc.* **2020**, *497*, 4981–4998. [CrossRef]

107. Rauscher, T.; Dauphas, N.; Dillmann, I.; Fröhlich, C.; Fülöp, Z.; Gyürky, G. Constraining the astrophysical origin of the p-nuclei through nuclear physics and meteoritic data. *Rep. Prog. Physics.* **2013**, *76*, 066201. [CrossRef] [PubMed]
108. Travaglio, C.; Rauscher, T.; Heger, A.; Pignatari, M.; West, C. Role of core-collapse supernovae in explaining solar system abundances of p nuclides. *Astrophys. J.* **2018**, *854*, 18–34. [CrossRef]
109. Heymann, D.; Dziczkaniec, M. Xenon from intermediate zones of supernovae. In Proceedings of the Lunar and Planetary Science Conference Proceedings, X 1979, #1943, Houston, TX, USA, 19–23 March 1979.
110. Howard, W.M.; Arnett, W.D.; Clayton, D.D.; Woosley, S.E. Nucleosynthesis of rare nuclei from seed nuclei in explosive carbon burning. *Astrophys. J.* **1972**, *175*, 201–216. [CrossRef]
111. Clayton, D.D. Origin of heavy xenon in meteoritic diamonds. *Astrophys. J.* **1989**, *340*, 613–619. [CrossRef]
112. Meyer, B.; Adams, D.C. Neutron burst production of 60Fe necessarily implies production of 182Hf. In Proceedings of the Lunar and Planetary Science Conference Proceedings, XXXVII 2006, #1403, League City, TX, USA, 13–17 March 2006.
113. Quitté, G.; Halliday, A.N.; Meyer, B.S.; Markowski, A.; Latkoczy, C.; Günther, D. Correlated iron 60, nickel 62, and zirconium 96 in refractory inclusions and the origin of the solar system. *Astrophys. J.* **2007**, *655*, 678–684. [CrossRef]